Supplementary Information for

Promoting electrocatalytic CO_2 methanation using a molecular modifier on Cu surfaces

Experimental Details

Chemicals and materials

1,2-Benzenethiol (BDT, >95.0%) was purchased from Aladdin Co. Ltd. (Shanghai, China). Copper (II) nitrate trihydrate (Cu $(NO_3)_2 \cdot 3H_2O$, >99.0%), copper (II) acetate, ethanol (C_2H_5OH, >99.5%), N, N-dimethylacetamide (DMF, >98.0%), toluene (C_7H_8, >98.0%), and hexane (C_6H_{14}, >96.0%), 1-amino-2-propanol (AmIP, > 98.0%), hydrazine monohydrate (H_6N_2O, >85.0%), potassium hydroxide (KOH, ≥99.5%) were purchased from Sinopharm Chemical Reagent Co. Ltd. (Shanghai, China). Nafion solution (~5% wt), ethylene glycol ($C_2H_6O_2$, ≥99.5%), 1-propanesulfonic acid 3-(trimethylsilyl) sodium salt (DSS), (methyl sulfoxide)-d_6 (DMSO-d_6), and Nafion 115 membranes were all purchased from Sigma-Aldrich. All the chemicals were used without further purification. Ultrapure Millipore water (resistivity 18.2 MΩ cm) was used for all experiments.

Synthesis of Cu nanoparticles (Cu NPs)

The Cu NPs were synthesized using a previously reported method with slight modification.[1] Typically, 15 mL of AmIP was added to 30 mL of ethylene glycol. Copper (II) acetate (2.73 g) was added to the AmIP solution in an ice bath, producing a blue solution. Then, hydrazine monohydrate (7.3 mL) was added to the blue solution under stirring at 800 rpm and room temperature. After the above reaction for around 24 h, blackish deep red products were collected by centrifugation and washed with DMF, toluene, and hexane.

Synthesis of Cu BDT

Cu $(NO_3)_2 \cdot 3H_2O$ (483.18mg, 2 mmol) and 1,2-Benzenedithiol (284.46 mg, 2 mmol) were dissolved in ethanol (5 mL) separately. Then, the solution of BDT was added to Cu $(NO_3)_2$ solution dropwise and stirred at room temperature, giving black powder (305.64 mg, 1.5 mmol, ~75% yield). The black solid was washed with ethanol and deionized water three times and was dried in an oven at 120 ℃ to obtain pure Cu BDT products.[2]

Preparation of the working electrode

3.2 mg of catalyst was dispersed in 2 ml of C_2H_5OH by sonicating for 10 minutes, and then 35 μL of Nafion solution (~5 wt.%) was added and sonicated for another 30 minutes to get a uniform ink. The obtained ink was spray-coated on 4 cm × 4 cm carbon paper (Sigracet 29BC). The prepared electrodes

were dried in the ambient environment. The prepared electrode was electrochemically reduced at a constant voltage of –1.5 V (vs Ag/AgCl) for 20 mins to obtain working electrode.

Electrochemical measurements

All CO_2 electroreduction experiments were carried out in a flow cell that was controlled by an electrochemical workstation (CHI 1140C). The anolyte and catholyte were pumped through the flow-cell devices using a peristaltic pump (BT100-2J, LONGER) at a flow rate of 50 rpm and separated by a proton exchange membrane (Nafion 115). As an electrolyte, 1 M KOH was used. The flow cell system's effective test area was 1×1 cm^2. The counter electrode and reference electrode were Pt wire and Ag/AgCl (3M KCl), respectively. The CO_2 flow rate was set at 20 sccm. All potentials were measured Ag/AgCl scale and converted to the RHE scale with *i*R compensation according to the following equation:

$$\mathrm{E\,(vs\ RHE)} = \mathrm{E\,(vs\ Ag/AgCl)} + 0.210\ \mathrm{V} + 0.059 \times \mathrm{pH} + iR$$

where i is the mean current at each applied potential and R is solution resistance determined by experiments of electrochemical impedance spectroscopy (EIS) in a frequency range from 10 to 10^6 Hz with an amplitude of 5 mV.

The quantitative methods of products in CO_2RR

The gaseous products of CO_2 electroreduction were analyzed by online gas chromatography (GC 2014, Shimadzu) equipped with a flame ionization detector (FID) and thermal conductivity detector (TCD). Faradaic efficiency (FE) of H_2, CO, C_2H_4, and CH_4 products were calculated following the equation:

$$\mathrm{FE}_{gas}\,(\%) = \frac{i_{\mathrm{gas}}}{i_{\mathrm{total}}} \times 100 = \frac{C_{\mathrm{gas}} \times V_{\mathrm{gas}} \times \frac{p_0}{RT} \times N \times F}{i_{\mathrm{total}}} \times 100$$

i_{gas} : the partial currents of gas products.

i_{total} : the total current was measured by the potentiostat.

C_{gas} : the volume concentration of gas products, based on the calibration of GC.

V_{gas} : flow rate of the input gas (95% CO_2, 5% N_2 as internal standard).

p_0 : atmospheric pressure.

R : ideal gas constant, 8.314 J mol^{-1} K^{-1}.

T : room temperature, 298.15 K.

N : the number of electrons transferred for the product formation.

F : Faraday constant, 96485 C mol^{-1}.

The liquid products were detected using ^{1}H NMR spectroscopy (AVANCE AV III 400, Bruker). Typically, 400 μL of the electrolyte after electrolysis was mixed with 100 μL DMSO-d_6 and 100 μL of 6.0 mM DSS aqueous solution. DSS solution serves as an internal standard. The area ratio of the liquid product peaks to the DSS peaks was compared to quantify the concentration of liquid products. The FE for the liquid product was calculated following the equation:

$$FE_{liquid}\,(\%) = \frac{C_{\text{liquid}} \times V_{\text{liquid}} \times N \times F}{Q_{\text{total}}} \times 100$$

C_{liquid} : concentration of the liquid product.

V_{liquid} : volume of the electrolyte.

Q_{total} : quantity of electric charge integrated by the potentiostat.

The calculated methods for the double-layer capacitance (C_{dl}) and electrochemical surface area (ECSA).

Double-layer capacitance (C_{dl}) was determined by measuring the capacitive current associated with double-layer charging from the scan-rate dependence of cyclic voltammogram (CV). The CV curves ranged from 0.825 V to 0.875 V vs RHE. The C_{dl} was estimated by plotting the Δj ($\Delta j = (j_a - j_c)/2$) at 0.85 V vs RHE against the scan rates, in which the j_a and j_c were the anodic and cathodic current density, respectively. The slope is that of the C_{dl} values. The ECSA was calculated by the following equation: ECSA = $R_f \times S$, where R_f represented the roughness factor of the Cu surface and S represented the surface area of the GDE (1 cm^2 in this case). Based on the C_{dl} of a smooth metallic surface (0.029 mF cm^{-2} for Cu surface),[3] R_f can be calculated according to the relation $R_f = C_{\text{dl}}/0.029$ in this case.

Evaluation of Yield Rate

The yield rate of gas or liquid product was calculated as follows:

$$Yield\ Rate_{gas/liquid} = \frac{i_{total} \times FE_{\text{gas/liquid}}}{N \times F \times S} \times 3600\ (s)$$

Computational methods

The CO_2 electroreduction on the benzenedithiol-modified Cu (111) surface was optimized by periodic DFT calculations using the Vienna Ab Initio Simulation Package (VASP).[4] The Perdew-Burke-Ernzerhof (PBE) functional and plane-wave basis set with a cutoff energy of 400 eV were selected for the calculations.[5] The ion-electron interaction was described using the projector-augmented plane wave (PAW) approach. A 5×5 supercell slab (14.2 Å×14.2 Å) was established for the bare Cu (111) and benzenedithiol-modified Cu (111) surface. The vacuum space along the Z direction was ~15 Å to avoid interaction between period images. The Brillouin zone was sampled by a 2×2×1 k points mesh. For structural optimization, the bottom two layers of the slab were fixed. At the same time, the rest atoms, including the Cu and adsorbates, were relaxed until the maximum force on the movable atoms was less than 0.02 eV $Å^{-1}$. Vibrational frequency was computed without imaginary frequency to verify whether the relaxed structure was minimum. The Gibbs free energy change is defined as $\Delta G = \Delta E + \Delta ZPE - TS$, where ΔE is obtained from DFT calculations, ΔZPE represents the corrections in zero-point energies from vibrational frequencies, ΔS is the change of entropy, and T is the absolute temperature. Entropy values of gaseous molecules and adsorbate are generated by the VASPKIT.[6] The reaction energies of *CO protonation and C–C coupling were calculated at 0 V_{RHE}.

Characterizations

X-ray diffraction patterns were recorded by using a Philips X'Pert Pro Super diffractometer with Cu-K_α radiation (λ = 1.54178 Å). The morphologies of samples were recorded by SEM (Zersss Supra 40) and TEM (Hitachi H-7650). HAADF-STEM and EDX mapping were taken on a field-emission transmission electron microscope (JEOL ARM-200F) operating at 200 kV accelerating voltage. The transmitted infrared spectra were carried out by Fourier transform-infrared spectroscopy (FT- IR) (Nicolet 8700). The amount of Cu loading in catalysts was determined by inductively coupled plasma atomic emission spectroscopy (ICP-AES) (Atom scan Advantage, Thermo Jarrell Ash, USA). X-ray

photoelectron spectroscopy (XPS) measurements were carried out on a VG ESCALAB MK II X-ray photoelectron spectrometer with an exciting source of Al K_α = 1486.6 eV. The binding energies were corrected for specimen charging by referencing C 1s to 284.6 eV. A contact angle analyzer (Attension Theta, Biolin Scientific) was used to measure the contact angle of samples.

In situ Raman measurements

We obtained in-situ Raman spectra of Cu NPs-BDT and Cu NPs under different potentials using an electrolytic cell with a three-electrode setup. The working electrode was made using the same procedure as described above but with Cu NPs-BDT as the catalyst. The counter electrode was a metal bar connected to a platinum wire going through the cell. The reference electrode was an Ag/AgCl electrode. Electrolytes containing 1 M KOH were cycled at a rate of 10 mL min^{-1}. During the CO_2RR, CO_2 gas was still flowing into the cell, a 785 nm laser was used to collect the catalyst surface directly, and a detector synchronously collected the Raman signals.

In situ ATR-SEIRAS measurements

An FT-IR spectrometer (Nicolet iS50, Thermo Scientific) equipped with an MCT-A detector was used to collect *in situ* ATR-SEIRAS data. 4 mg of electrocatalysts, 180 μL of C_2H_5OH, and 20 μL of Nafion were combined to make the catalyst ink. The ink solution was then dripped onto the central portion of an Au film that had been chemically deposited on the basal plane of a hemicylindrical Si prism. The Si prism was built in an electrochemical cell with a Pt wire counter electrode, an Ag/AgCl electrode as a reference electrode, and 0.1 M $KHCO_3$ solution as electrolytes. Each single-beam scope had an average of 64 scans, and all spectra were acquired at a resolution of 4 cm^{-1}. For potential control, an electrochemical workstation (CHI 660E) was used. Throughout the reaction, high-purity CO_2 gas was continually introduced into the electrolytes.

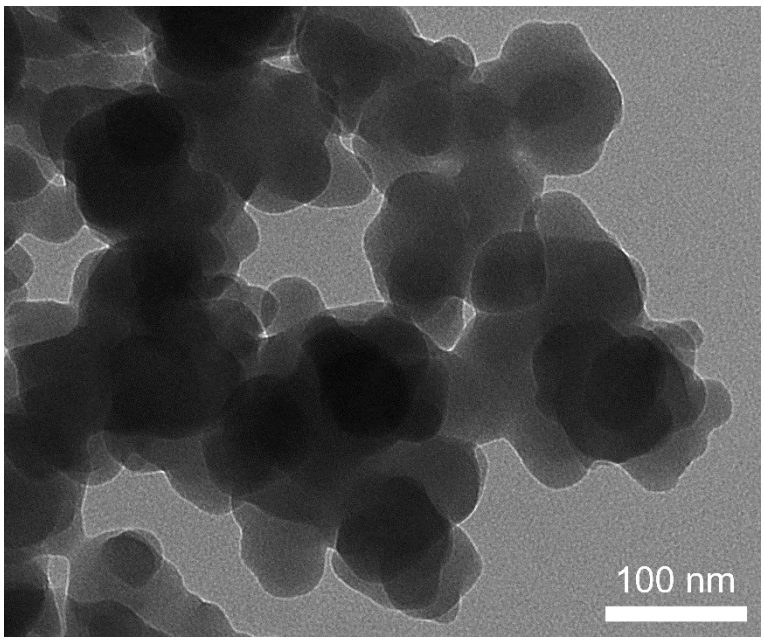

Figure S1. TEM of the precursor Cu BDT.

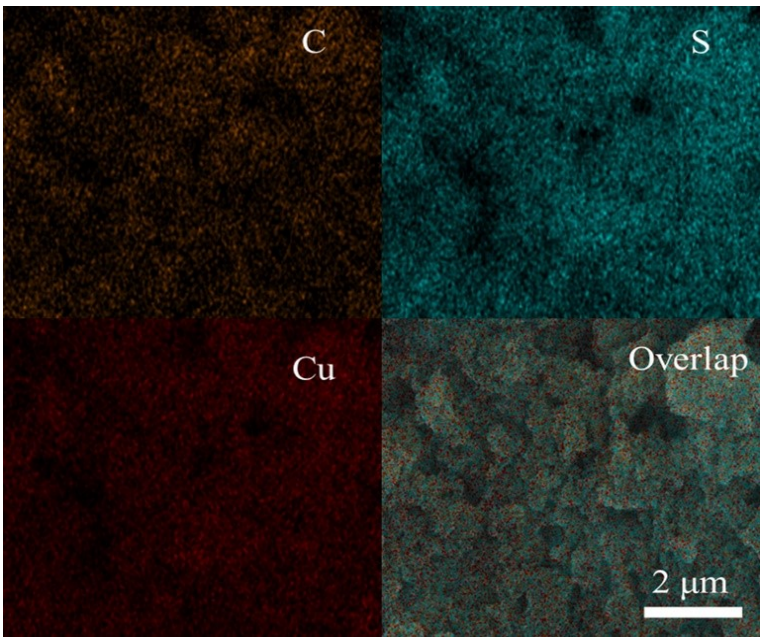

Figure S2. EDX mapping of the precursor Cu BDT.

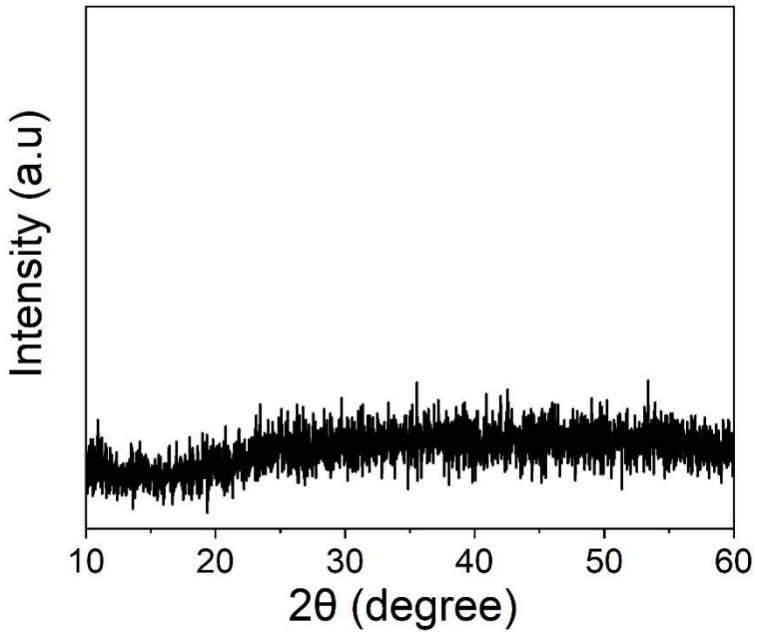

Figure S3. XRD patterns of the precursor Cu BDT.

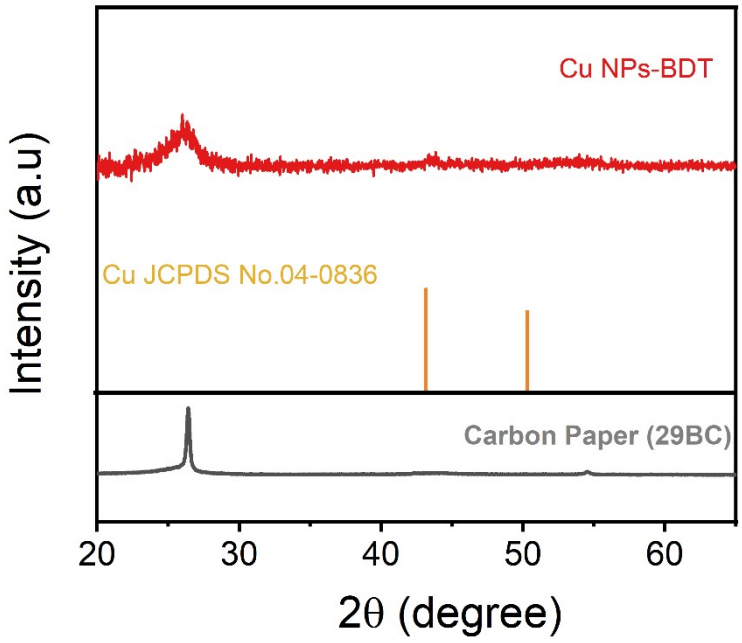

Figure S4. XRD patterns of Cu NPs-BDT.The prominent peaksaround 26.0° and 43.6° are assigned to the carbon peaks of 29 BC Carbon paper support.

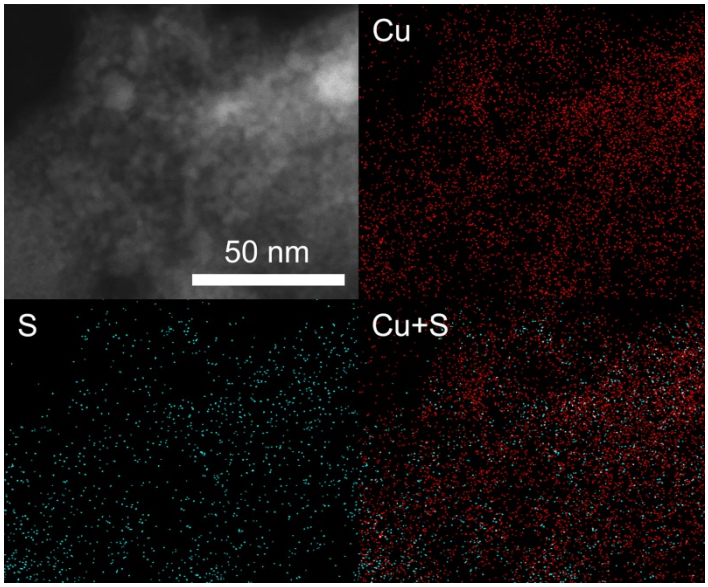

Figure S5. EDX mapping of BDT modified Cu NPs (Cu NPs-BDT).

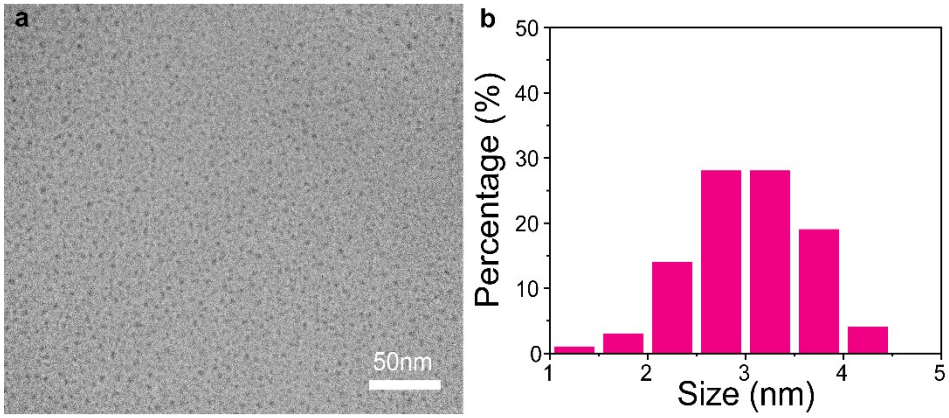

Figure S6. (a) TEM images of Cu nanoparticles (Cu NPs) and (b) particle size distribution of Cu NPs.

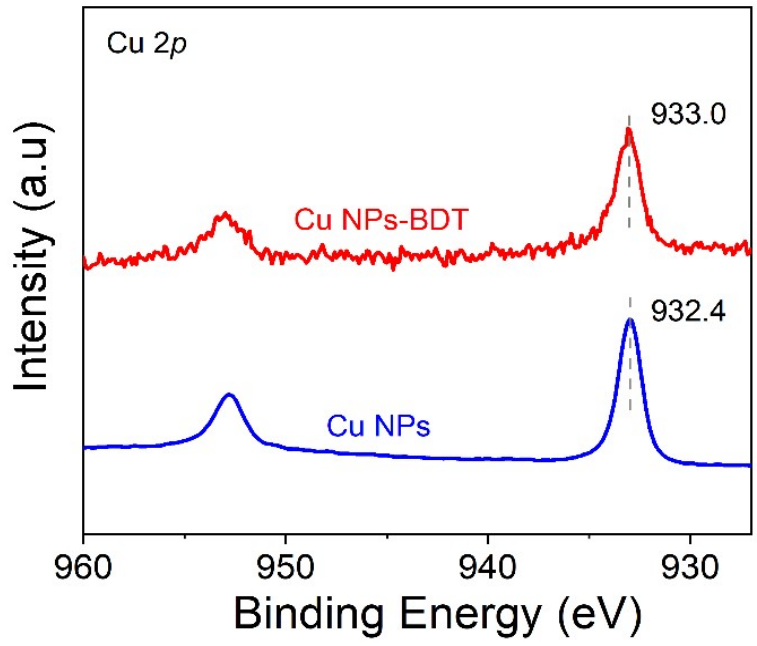

Figure S7. High-resolution Cu 2p spectra of Cu NPs-BDT and Cu NPs.

1 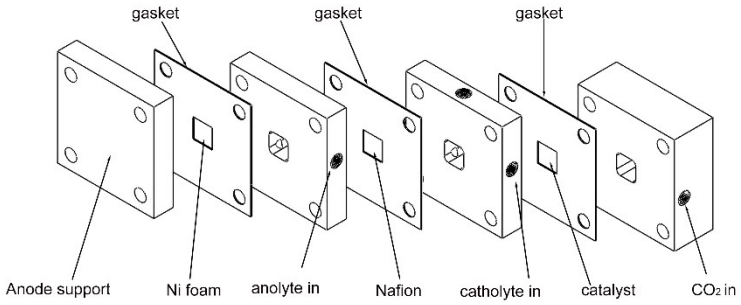

2 **Figure S8.** Illustration of the flow cell setup.

3

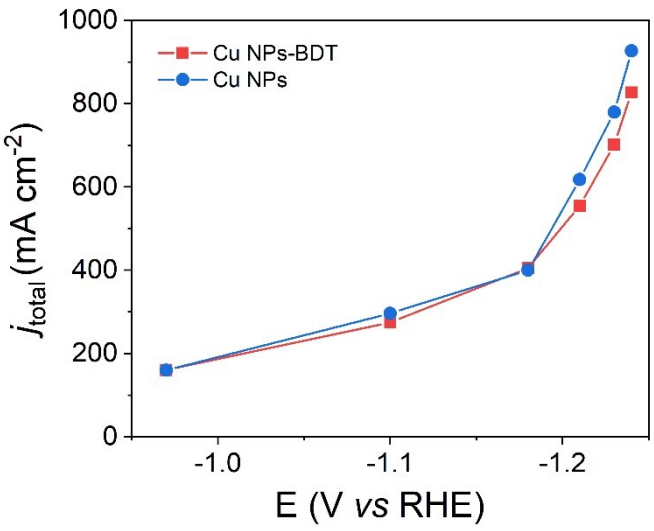

Figure S9. Chronoamperometric curves at various potentials for CO_2 reduction on (a) Cu NPs-BDT and (b) Cu NPs in 1 M KOH electrolyte, respectively.

1 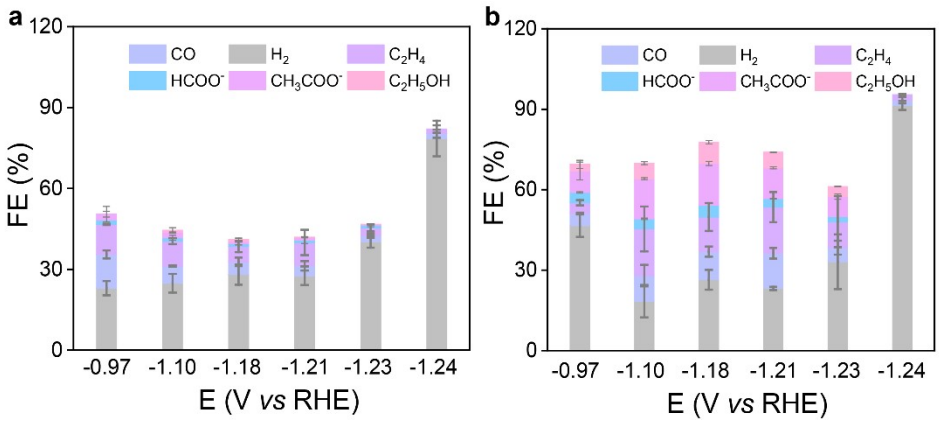

2 **Figure S10.** FEs of H_2, CO, $HCOO^-$, CH_3COO^-, C_2H_5OH toward CO_2RR at different Voltages from
3 -0.97 V to -1.24 V (Vs RHE) on (a) Cu NPs-BDT and (b) Cu NPs.
4

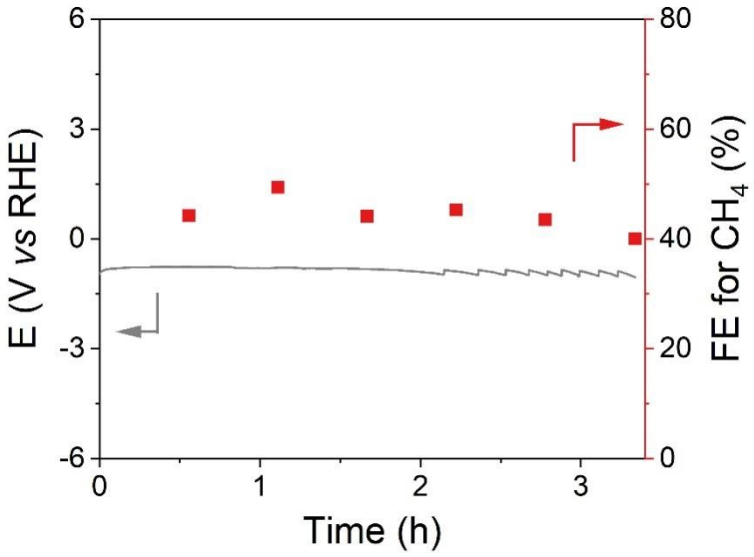

Figure S11. Plot of the voltage Performance test of CO_2RR to methane during 3.3 hours of electrolysis under the current density of 200 mA cm^{-2} at 1M KOH.

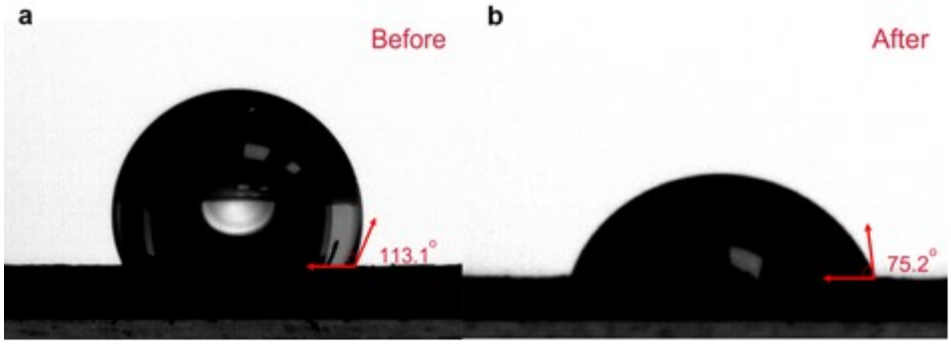

Figure S12. The contact angle measurements on the back side of the gas diffusion layer that was used to support the catalysts (a) before CO_2RR and (b) after 3.3-h electrolysis.

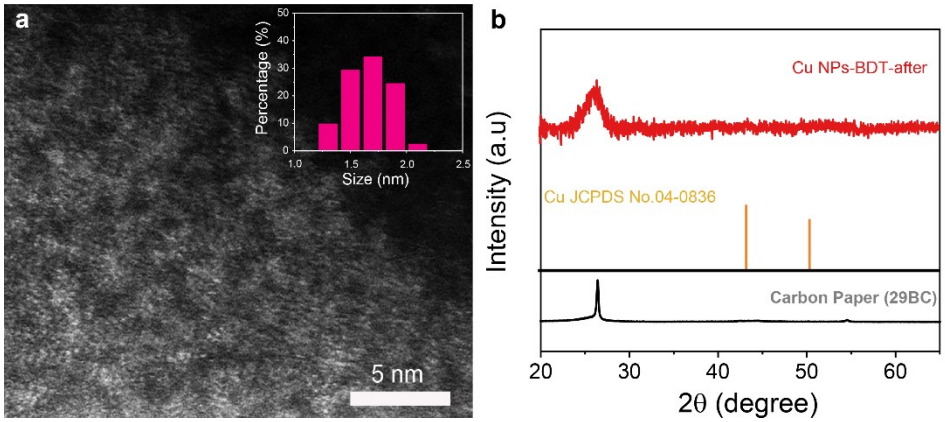

Figure S13. (a) High-resolution STEM of Cu NPs-BDT and (b) XRD pattern of Cu NPs-BDT after after 3.3-h electrolysis.

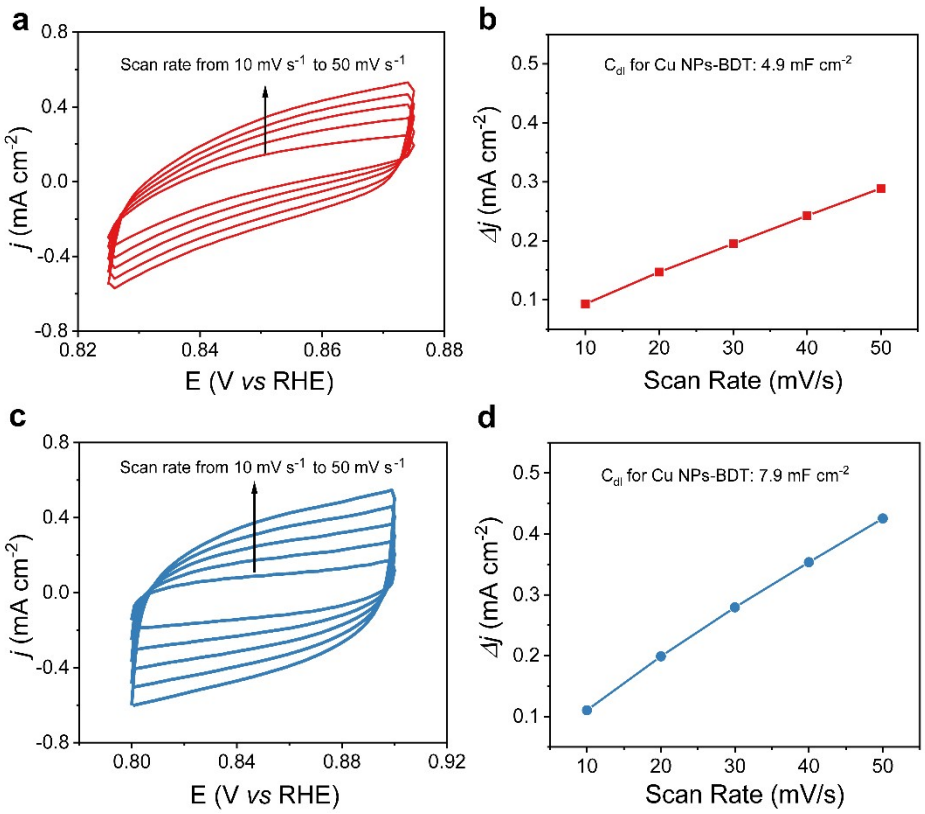

1

2 **Figure S14.** CV curves (a) and charge current density differences (Δj) plotted against scan rates (b)

3 for Cu NPs-BDT.CV curves (c) and Δj plotted against scan rates (d) for Cu NPs.

4

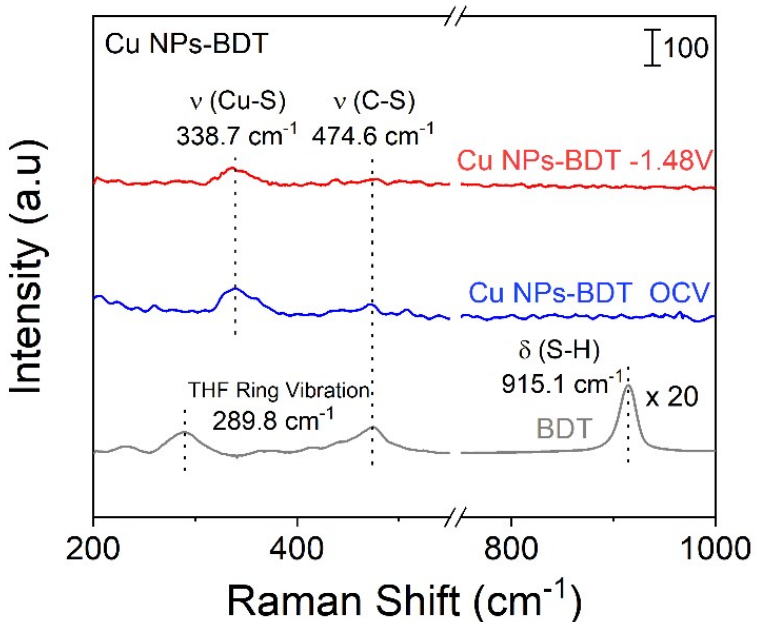

Figure S15. *In situ* Raman spectra of Cu NPs-BDT were measured in 1 M KOH with a modified liquid-electrolyte flow rate. The peaks at 338.7 cm^{-1}, 474.6 cm^{-1}, and 915.1 cm^{-1} was attributed to the Cu–S, C–S, and S–H stretching vibrations on the benzene ring, respectively.[7,8] Meanwhile, the peak at 289.8 cm^{-1} was attributed to the ring's vibration of tetrahydrofuran (THF).[9]

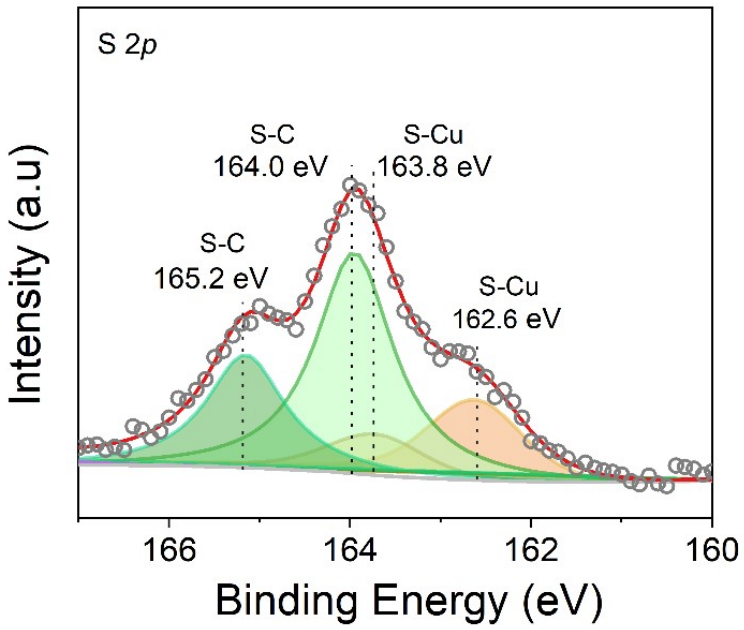

Figure S16. High-resolution XPS spectra of S 2p peaks of Cu NPs-BDT after 3.3-h electrolysis.

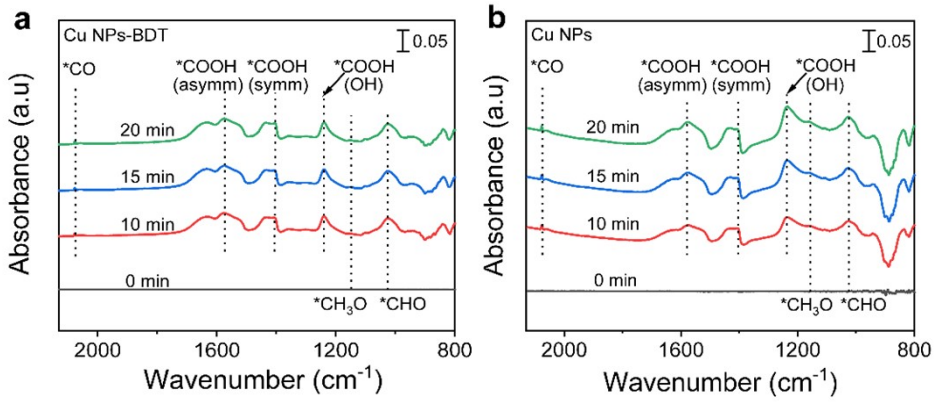

Figure S17. *In-situ* ATR-SEIRAS spectra toward CO_2 electroreduction over (a) Cu NPs-BDT and (b) Cu NPs at -0.87 V vs RHE. The peaks at 1240 cm^{-1}, 1404 cm^{-1}, and 1574 cm^{-1} could be attributed to the OH deformation (*COOH), symmetric stretch, and asymmetric stretch of the *COOH group, respectively.[10–13] Meanwhile, the signals that appeared at 1027 cm^{-1}, 1155 cm^{-1}, and 2078 cm^{-1} might be assigned to *CHO, *OCH_3, and *CO intermediate. [10–15]

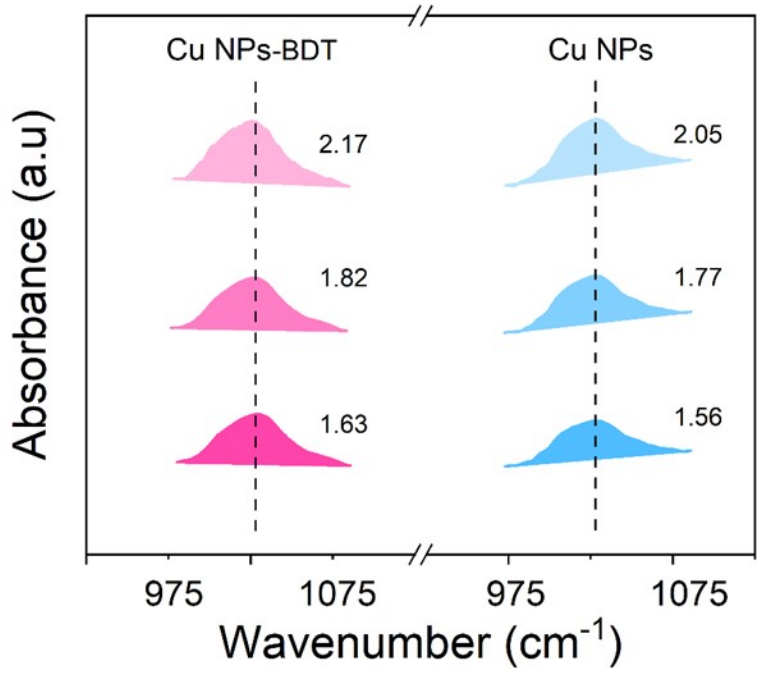

Figure S18. Integrated *CHO peak areas in in situ ATR-SEIRAS spectra of Cu NPs-BDT and Cu NPs at -0.87 V vs RHE for 10 min,15 min, and 20 min.

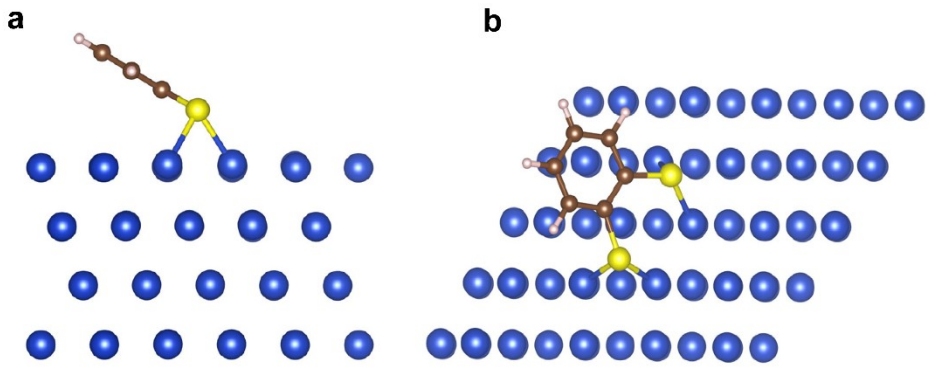

Figure S19. (a) Side view and (b) top view images of the optimized configuration of BDT-modified Cu (111) Slab. Blue, dark yellow, brown, and pink balls stand for copper, sulfur, carbon, and hydrogen atoms, respectively.

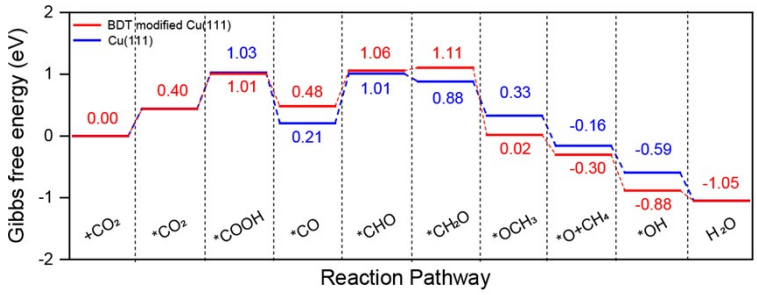

1

2 **Figure S20.** The Gibbs free energies of CO_2-to -CH_4 pathway on Cu (111) slab and BDT-modified

3 Cu (111) slab under the surface coverage of 1/36 ML *CO .

4

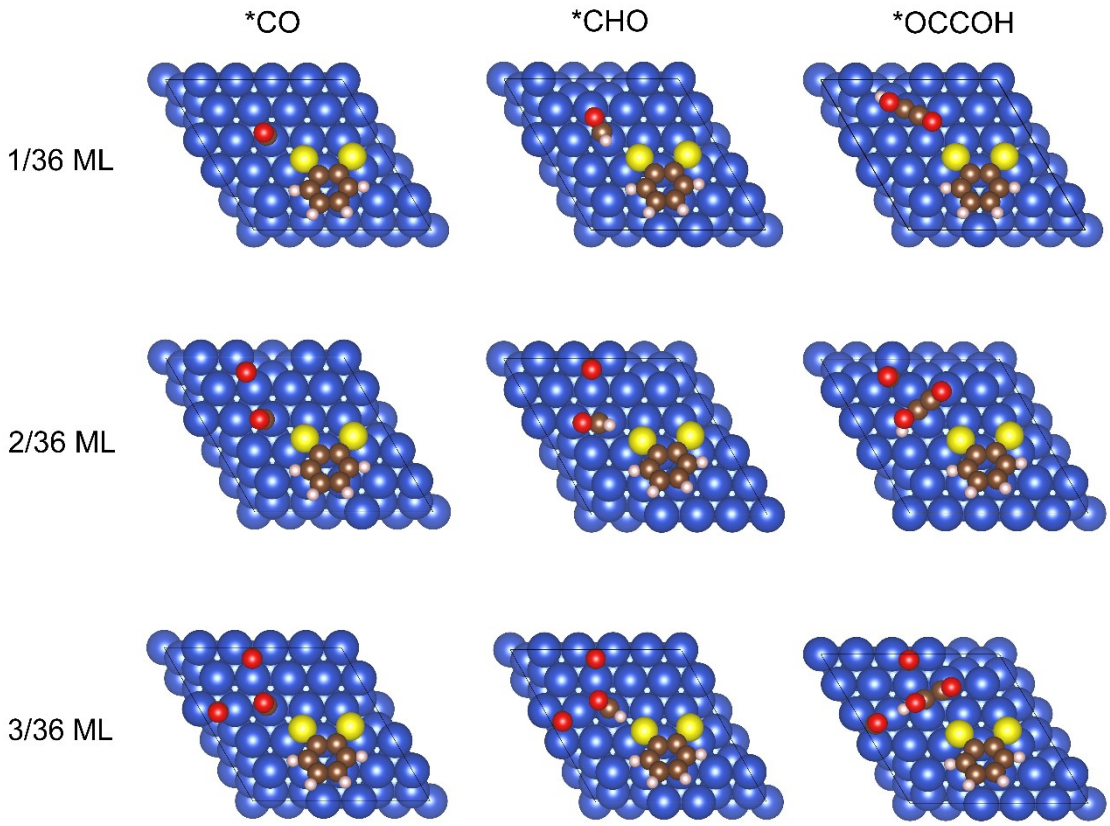

Figure S21. Adsorption configurations of *CO, *CHO, and *OCCO on BDT modified Cu (111) surface with different *CO coverages. Blue, dark yellow, red, brown, and pink balls stand for copper, sulfur, oxygen, carbon, and hydrogen atoms, respectively.

Table S1. The amount of Cu loading in as-prepared Cu NPs-BDT investigated by ICP-AES.

Catalyst	Cu (w.t.%)
Cu NPs-BDT	~9.8

Table S2. Peak areas normalized by ECSA for *CO with adsorption in *in situ* ATR-SEIRAS spectra under the voltage of -0.87V vs RHE at different times.

Peak areas / Catalyst	10 min	15 min	20 min
Cu NPs-BDT	0.71×10^{-4}	0.77×10^{-4}	0.89×10^{-4}
Cu NPs	1.69×10^{-4}	1.76×10^{-4}	1.80×10^{-4}

Table S3. Peak areas normalized by ECSA for *CHO with adsorption in *in situ* ATR-SEIRAS spectra under the voltage of -0.87V vs RHE at different times.

Peak areas / Catalyst	10 min	15 min	20 min
Cu NPs-BDT	0.33	0.37	0.44
Cu NPs	0.20	0.22	0.25

References

1. Y. Hokita, M. Kanzaki, T. Sugiyama, R. Arakawa and H. Kawasaki, *ACS Appl. Mater. Interfaces*, 2015, **7**, 19382–19389.
2. F. Li, W. Guo, Y. Si, Z. Li and Y. Fu, *Electrochim. Acta*, 2021, **370**, 137757.
3. F. Li, Y. C. Li, Z. Wang, J. Li, D.-H. Nam, Y. Lum, M. Luo, X. Wang, A. Ozden, S.-F. Hung, B. Chen, Y. Wang, J. Wicks, Y. Xu, Y. Li, C. M. Gabardo, C.-T. Dinh, Y. Wang, T.-T. Zhuang, D. Sinton and E. H. Sargent, *Nat. Catal.*, 2020, **3**, 75–82.
4. G. Kresse and J. Furthmüller, *Phys. Rev. B*, 1996, **54**, 11169–11186.
5. J. P. Perdew, K. Burke and M. Ernzerhof, *Phys. Rev. Lett.*, 1996, **77**, 3865–3868.
6. V. Wang, N. Xu, J.-C. Liu, G. Tang and W.-T. Geng, *Comput. Phys. Commun.*, 2021, **267**, 108033.
7. T. Y. K. William P. Griffith, *Spectrochim. Acta, Part A*, 1995, **51**, 253–267.
8. C. R. Andrew, H. Yeom, J. S. Valentine, B. G. Karlsson, G. van Pouderoyen, G. W. Canters, T. M. Loehr, J. Sanders-Loehr and N. Bonander, *J. Am. Chem. Soc.*, 1994, **116**, 11489–11498.
9. B. Cadioli, E. Gallinella, C. Coulombeau, H. Jobic and G. Berthier, *J. Phys. Chem.*, 1993, **97**, 7844–7856.
10. J.-D. Yi, R. Xie, Z.-L. Xie, G.-L. Chai, T.-F. Liu, R.-P. Chen, Y.-B. Huang and R. Cao, *Angew. Chem. Int. Ed.*, 2020, **59**, 23641–23648.
11. X. Li, Y. Sun, J. Xu, Y. Shao, J. Wu, X. Xu, Y. Pan, H. Ju, J. Zhu and Y. Xie, *Nat. Energy*, 2019, **4**, 690–699.
12. S. Chen, W.-H. Li, W. Jiang, J. Yang, J. Zhu, L. Wang, H. Ou, Z. Zhuang, M. Chen, X. Sun, D. Wang and Y. Li, *Angew. Chem. Int. Ed.*, 2021, anie.202114450.
13. Y. Wang, M. Liu, G. Gao, Y. Yang, R. Yang, H. Ding, Y. Chen, S. Li and Y. Lan, *Angew. Chem. Int. Ed.*, 2021, **60**, 21952–21958.
14. N. J. Firet and W. A. Smith, *ACS Catal.*, 2017, **7**, 606–612.
15. S. Zhu, T. Li, W.-B. Cai and M. Shao, *ACS Energy Lett.*, 2019, **4**, 682–689.